Mechanical Systems and Signal Processing 107 (2018) 484–501

Contents lists available at ScienceDirect

Mechanical Systems and Signal Processing

journal homepage: www.elsevier.com/locate/ymssp

A neural network-based input shaping for swing suppression of an overhead crane under payload hoisting and mass variations

Liyana Ramli [a], Z. Mohamed [a,*], H.I. Jaafar [a,b]

[a] Faculty of Electrical Engineering, Universiti Teknologi Malaysia, Johor, Malaysia
[b] Faculty of Electrical Engineering, Universiti Teknikal Malaysia Melaka, Melaka, Malaysia

ARTICLE INFO

Article history:
Received 16 October 2017
Received in revised form 22 December 2017
Accepted 18 January 2018

Keywords:
Hoisting
Input shaping
Neural network
Overhead crane
Swing suppression

ABSTRACT

This paper proposes an improved input shaping for minimising payload swing of an overhead crane with payload hoisting and payload mass variations. A real time unity magnitude zero vibration (UMZV) shaper is designed by using an artificial neural network trained by particle swarm optimisation. The proposed technique could predict and directly update the shaper's parameters in real time to handle the effects of time-varying parameters during the crane operation with hoisting. To evaluate the performances of the proposed method, experiments are conducted on a laboratory overhead crane with a payload hoisting, different payload masses and two different crane motions. The superiority of the proposed method is confirmed by reductions of at least 38.9% and 91.3% in the overall and residual swing responses, respectively over a UMZV shaper designed using an average operating frequency and a robust shaper namely Zero Vibration Derivative-Derivative (ZVDD). The proposed method also demonstrates a significant residual swing suppression as compared to a ZVDD shaper designed based on varying frequency. In addition, the significant reductions are achieved with a less shaper duration resulting in a satisfactory speed of response. It is envisaged that the proposed method can be used for designing effective input shapers for payload swing suppression of a crane with time-varying parameters and for a crane that employ finite actuation states.

1. Introduction

Vibration/oscillation suppression is the main issue in controlling a flexible structure and under-actuated mechanical system such as cranes. An overhead crane is widely used in loading ship cargoes, transporting heavy loads in various industrial factories and handling nuclear waste, which such applications require low payload oscillation during motion. Commonly, most of the crane operations are conducted manually, which lead to many drawbacks such as long operation required to compensate the swing, safety issues and inaccurate load positioning. In practice, hoisting is an essential operation for loading, positioning and unloading of various payloads. Therefore, cranes tend to suffer from uncertainties due to changes in cable length and payload mass. This results in a dynamic modelling error and designing of controllers is challenging as the damping ratio and natural frequency ought to change during the hoisting operation [1].

There are various strategies that could be applied for crane control and these can be categorised into closed-loop and open loop control techniques. A latest review regarding control strategies of crane systems was discussed in [2]. Open loop

* Corresponding author.
E-mail address: zahar@fke.utm.my (Z. Mohamed).

https://doi.org/10.1016/j.ymssp.2018.01.029
0888-3270/

strategies are very known with its capability as a swing control and these include input shaping control [3–11], filter [12,13] and command smoothing [14–16]. Besides, closed-loop strategies have been implemented pervasively to surmount these issues. Enormous publications regarding closed-loop control methods including linear control [17,18], sliding mode control [19,20], model predictive control [21,22], generalised predictive control [23], adaptive control [24,25] and fuzzy logic control [26,27] were designed for position control with swing suppression for cranes. Recently, Sun et al. [28] proposed an energy-optimal planner for a double pendulum crane system that focused on suppressing the swing angles while minimising the energy consumption.

Basically, input shaping requires a priori knowledge of system parameters such as natural frequency and damping ratio for designing the amplitudes and time locations of the impulses to achieve an effective shaper design. This is highly depending on the model accuracy to yield a good design of input shaper in restraining the vibration. Practically, the zero vibration (ZV) shaper was effective but limited for the applications that system parameters did not change significantly [29]. The main drawback of this technique is that it is sensitive towards the existence of parameter variations [2]. Since then, several input shapers have been proposed and designed that were robust and less sensitive to modelling errors such as zero vibration derivative (ZVD), Zero Vibration Derivative-Derivative (ZVDD), Zero Vibration Derivative-Derivative-Derivative (ZVDDD), Extra-insensitive (EI) and Specified-Insensitivity (SI). However, improvements in robustness of these types of input shapers lead to an increase in a rise time [29] as more constraints are added and resulted in a longer shaper.

Another issue in input shaping that is studied is to include an adaptive mechanism that can update the shaper parameters for a system with changing parameters. An adaptive input shaping was proposed in [30] to make use of the shorter input shaper (i.e., ZV shaper) that is fast in rise time and make it insensitive/robust towards parameter variations. A frequency domain identification method was proposed by Tzes and Yurkovich [31] to estimate the frequency in real time, but it was computational burden due to an FFT analysis during the control calculation. Time domain identification was proposed in [32] and iterative learning scheme for input shaping in [33]. On the other hand, since the effect of hoisting is one of the crucial factors to be considered in adaptive shaper design for restraining the payload swing, Singhose et al. [1] investigated the effect of hoisting on the input shaping control and proposed input shapers based on the average operating frequency (AOF). The results showed a better improvement in payload swing suppression as compared to the shapers that were based on an initial frequency.

Typically, cranes employ relay-driven drives that actuate the system with finite actuation states. For instance, the crane can only be operated under the following states: off, slow and fast motions. In this case, one of the most appropriate types of input shaper that resembles the finite actuated oscillatory system is called a unity magnitude zero vibration (UMZV) shaper. The performance of UMZV shaper is less affected than ZV and ZVD shapers when a less number of admissible actuation states was used [34]. Besides, the unity magnitude shapers have less shaper duration as compared to the shapers comprising all positive impulses such as the ZV shaper [35]. For the undamped system, the analytical solution for the UMZV shaper can be derived as in [36]. However, finding a closed-form solution of the UMZV shaper for a damped system is difficult and the input shaper tend to change with respect to the damping ratio. Besides, the insensitivity of this shaper is weak when dealing with the variation in natural frequency of the system. Gürleyük [35] designed a new set of solution for UMZV that was applicable for all exact values of damping ratio and natural frequency of the system to yield a reasonable level of residual vibration. The other implementations of UMZV shaper have been proposed in [34,37,38] for flexible systems. However, most of the UMZV shapers were designed for a crane system with a fixed cable length and payload mass. As hoisting is an essential operation and a payload mass may vary, a scheme that can update the shaper parameters for a uniform system performance is desirable.

In this paper, an improved shaper that can predict and update the UMZV shaper parameters during payload hoisting and under payload mass variations for a low payload swing of the crane is proposed. The improved shaper is developed using an artificial neural network (ANN) that provides a nonlinear input–output mapping for important variables to yield an accurate shaper design. In this work, experiments using a laboratory overhead crane system are conducted to evaluate the performances of the proposed ANN-UMZV shaper. The transient, residual and overall payload swing performances are analysed under two practical cases involving different crane motions and payload hoisting. The UMZV shaper that utilises AOF scheme, and ZVDD shapers based on fixed and varying frequencies are also implemented for performance comparisons. The ZVDD shapers are considered as robust shapers. The main contribution of this paper lies on the design of an improved UMZV shaper that can predict and directly update the shaper parameters in real-time for a low payload swing during payload hoisting and changes in the payload mass. As the proposed UMZV shaper can provide a significant payload swing suppression under those effects together with a less shaper duration, the shaper provides a better performance than a robust shaper.

2. Model description

Fig. 1 shows a laboratory overhead crane used for verifications of controllers in this work. The length, height and width of the crane are 1.0 m each. The crane is equipped with a motion mechanism driven by a DC motor, while three measuring encoders with a resolution of 4096 pulses per rotation are used for measuring the trolley position, the cable length and the payload angle. The payload angle can be measured with an accuracy of 0.0015 rad. A Pentium-based personal computer was used and the control algorithm was realised using the MATLAB/Simulink. Table 1 shows the system parameters for the laboratory overhead crane.

Fig. 1. An overhead crane with payload.

Table 1
System parameters.

System parameters	Values
Hoisting cable length, l	0.17–0.59 m
Gravitational constant, g	9.8 ms^{-2}
Viscous damping coefficients, b_x, b_l	82, 75 Ns/m
Mass of payloads, m	0.74 kg, 0.24 kg
Mass of trolley, m_r	1.155 kg

Fig. 2 shows the plane model of a two-dimensional (2-D) overhead crane with a payload attached to the cable. A distance r indicates a path taken by the trolley as it moves from the origin, up to the suspension point of the cable on the trolley. l, m and θ denote the hoisting cable length, payload mass and swing angle, respectively. f_r and f_l denote the driving forces for r and l motions, respectively. The equations of motion of the crane system can be obtained as

$$(m_r + m)\ddot{r} + ml\cos\theta\ddot{\theta} + m\sin\theta\ddot{l} + b_x\dot{r} + 2m\cos\theta\dot{l}\dot{\theta} - ml\sin\theta\dot{\theta}^2 = f_r \tag{1}$$

$$m\ddot{l} + m\sin\theta\ddot{r} + b_l\dot{l} - ml\dot{\theta}^2 - mg\cos\theta = f_l \tag{2}$$

$$ml^2\ddot{\theta} + ml\cos\theta\ddot{r} + 2ml\dot{l}\dot{\theta} + mgl\sin\theta = 0 \tag{3}$$

where m_r is the travelling components of crane mass that includes the equivalent masses of the rotating parts, g is the gravitational acceleration, and b_x and b_l represent the viscous damping coefficients for the r and l motions, respectively. The mass

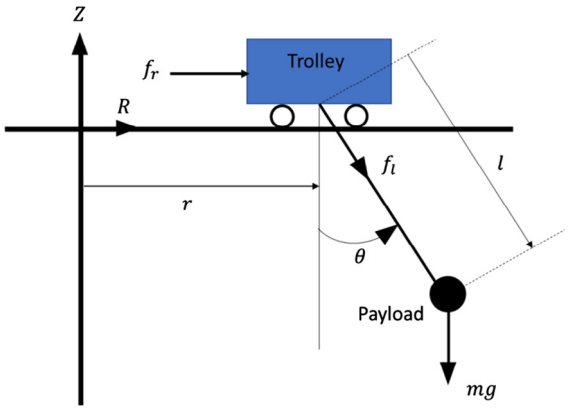

Fig. 2. Plane model of a two-dimensional overhead crane with hoisting payload.

and stiffness of the cable and the viscous damping in the payload swing are neglected and the payload is considered as a point mass.

3. Input shaping

Input shaping is an effective technique for reducing vibration of a flexible system. The main idea of the input shaping design in cancelling of the system vibrations is by applying a sequence of impulses to the system so as to cancel the vibration made by the first impulse. To have a good design of the input shaper, exact values of natural frequency ω_n and damping ratio ζ are required.

3.1. Zero Vibration Derivative-Derivative (ZVDD) shaper

The residual vibration that results from a series of impulses is given as

$$V(\omega,\zeta) = e^{-\zeta\omega t_n}\sqrt{C(\omega,\zeta)^2 + S(\omega,\zeta)^2} \tag{4}$$

where

$$\begin{aligned} C(\omega,\zeta) &= \sum_{i=1}^{n} A_i e^{-\zeta\omega t_i}\cos\left(\omega_n\sqrt{1-\zeta^2}t_i\right) \\ S(\omega,\zeta) &= \sum_{i=1}^{n} A_i e^{-\zeta\omega t_i}\sin\left(\omega_n\sqrt{1-\zeta^2}t_i\right) \end{aligned} \tag{5}$$

A_i and t_i denote the amplitudes and time locations of the impulses, and n is the number of impulses in the impulse series. To achieve a zero-residual vibration, Eq. (4) is set to zero. Moreover, some constrains need to be applied on the impulse amplitudes to avoid from infinite or zero values of the impulses. The constraint is added such that the sum of the impulse amplitudes is set to one, given as

$$\sum_{i=1}^{n} A_i = 1 \tag{6}$$

By solving Eqs. (4)–(6), where $V(\omega,\zeta)$ is equal to zero, the impulse amplitudes and time locations of a two-impulse shaper known as ZV shaper can be obtained. The effectiveness of the input shaping depends on the impulse amplitude and time locations designed based on the system parameters (ω_n and ζ). Hence, the error in obtaining these parameters could induce a higher vibration even with a small modelling error. The robustness of input shaper can be enhanced by considering the derivative of $V(\omega,\zeta) = 0$ with respect to ω_n, which is called the ZVD shaper. Further, a more robust shaper known as ZVDD can be obtained with the second derivative, where the impulse amplitudes and time locations [39] can be calculated as

$$\begin{bmatrix} A_i \\ t_i \end{bmatrix} = \begin{bmatrix} \frac{1}{(1+K)^3} & \frac{3K}{(1+K)^3} & \frac{3K^2}{(1+K)^3} & \frac{K^3}{(1+K)^3} \\ 0 & \pi/\omega_d & 2\pi/\omega_d & 3\pi/\omega_d \end{bmatrix} \tag{7}$$

and

$$K = \exp\left(\frac{-\zeta\pi}{\sqrt{1-\zeta^2}}\right);\ \omega_d = \omega_n\sqrt{1-\zeta^2}$$

Fig. 3 shows the shaping process of the ZVDD shaper that involves a convolution of an input command with sequence of impulses. The shaped input is then applied to a system in an open loop configuration for suppression of the system vibration. For a system with varying frequencies, input shapers that can be updated based on the new frequency can be designed. In particular for a crane system, a cable length which is related to the swing frequency can be measured and used to design the input shaper. This technique is further discussed in Section 5.

3.2. Unity-Magnitude Zero vibration (UMZV) shaper

Apart from utilising ZV-type shapers that contain positive impulse amplitudes, a shorter shaper could be obtained if negative impulse amplitudes are considered [34,35]. This is due to the impulse amplitudes that are constrained to be 1 or −1 to achieve a time-optimal command. This constraint is designed in conjunction with Eqs. (4)–(6) to produce the UMZV shaper given as [34,35]

$$\begin{bmatrix} A_i \\ t_i \end{bmatrix} = \begin{bmatrix} 1 & -1 & 1 \\ 0 & t_2 & t_3 \end{bmatrix} \tag{8}$$

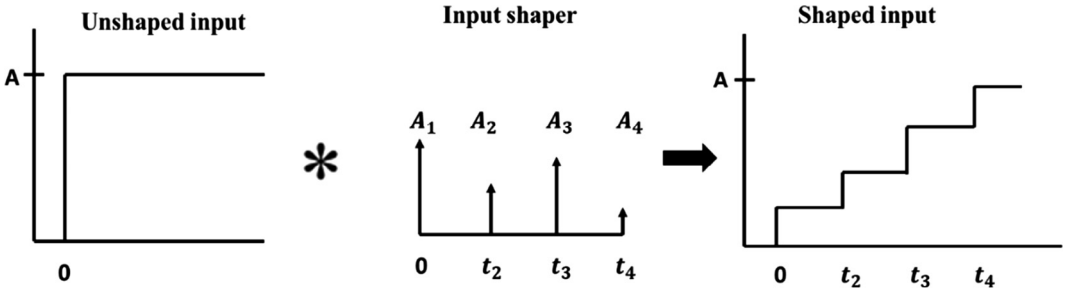

Fig. 3. ZVDD shaping process.

where

$$\begin{bmatrix} t_2 \\ t_3 \end{bmatrix} = \begin{bmatrix} 2\pi/\omega_d(1/6 + 0.272\zeta + 0.203\zeta^2) \\ 2\pi/\omega_d(1/3 + 0.005\zeta + 0.179\zeta^2) \end{bmatrix} \tag{9}$$

In this paper, since finding the closed-form solution of UMZV shaper for damped systems with time-varying parameters is difficult, the optimal time locations of the UMZV were obtained by using the particle swarm optimisation (PSO) algorithm as proposed by Maghsoudi et al. [11]. The PSO is utilised via simulation to find optimal shaper's parameters to yield the lowest swing angle for the system. The performance index based on the integral absolute error (IAE), $I(e)$ was considered as a fitness function, given as

$$I(e) = \int_0^\infty |\theta_d - \theta| dt \tag{10}$$

where θ and θ_d are the actual and desired swing angles respectively. The fitness value was calculated at each iteration of the PSO to finally find the optimal shaper's parameters. The optimisation process was carried out to find all the optimal shaper's parameters by using simulation in MATLAB and the results are as tabulated in Table 2. Payload masses of between 0.2 kg and

Table 2
Optimal UMZV shaper's parameters.

Sample no.	Payload mass (kg)	Cable length (m)	t_2 (s)	t_3 (s)
1	0.2	0.1	0.1089	0.2171
2	0.2	0.2	0.1484	0.3002
3	0.2	0.3	0.186	0.3724
4	0.2	0.4	0.2121	0.4246
5	0.2	0.5	0.2358	0.4729
6	0.2	0.6	0.2621	0.5229
7	0.4	0.1	0.108	0.2158
8	0.4	0.2	0.1507	0.3028
9	0.4	0.3	0.1899	0.373
10	0.4	0.4	0.2119	0.4242
11	0.4	0.5	0.2352	0.473
12	0.4	0.6	0.2582	0.5227
13	0.6	0.1	0.11	0.2179
14	0.6	0.2	0.1489	0.3026
15	0.6	0.3	0.19	0.3726
16	0.6	0.4	0.2089	0.4234
17	0.6	0.5	0.2289	0.4703
18	0.6	0.6	0.258	0.5226
19	0.8	0.1	0.1089	0.218
20	0.8	0.2	0.153	0.3027
21	0.8	0.3	0.1899	0.373
22	0.8	0.4	0.2081	0.4235
23	0.8	0.5	0.2081	0.4235
24	0.8	0.6	0.2698	0.5228
25	1	0.1	0.1135	0.2195
26	1	0.2	0.148	0.3
27	1	0.3	0.19	0.373
28	1	0.4	0.212	0.4233
29	1	0.5	0.232	0.4676
30	1	0.6	0.2814	0.542

1 kg and different cable lengths of between 0.1 m and 0.6 m were considered. The ranges of both the payload mass and cable length correspond to the limitations of the laboratory crane, which can perform a hoisting up to 0.6 m and carry a maximum of 1 kg payload.

4. ANN-based UMZV shaper design for real time implementation

This section describes the application of ANN for designing a real time UMZV shaper. The use of ANN in the development of intelligent control scheme has become a major role where it can either be used for system identification or as controller parameterisation [40]. The interconnected neurons in the ANN resembles the functionality of the human brain system. One of the advantages associated with ANN is the capability of adapting to a new environment or ability to learn when a complete formulation is unknown [41].

The traditional input shaping scheme is derived using a linear second order system and work effectively for suppressing oscillation in linear plants. However, the input-shaped signal could not provide a similar performance for nonlinear systems. Hence, a new technique in finding optimal shaper parameters is needed, and it is envisaged that a metaheuristic method could be utilised to achieve the objective. The optimal shaper's parameters as shown in Table 2 were obtained based on a nonlinear model utilising the PSO algorithm for various cable lengths and payload masses. However, for a real time implementation, it is difficult to use heuristic optimisation methods including PSO as they are usually utilised for an offline optimisation [42]. Hence, the ANN is proposed in this paper due to its benefit for real time prediction. The collected input and output data as shown in Table 2 was used for the training and to construct ANN nonlinear mapping between the inputs (cable length and payload mass) and the shaper parameters. Thus, the UMZV shaper can be updated online for any cable length and payload mass as shown in Fig. 4. This work assumes that the payload mass and cable length are measurable. This is common especially for industrial cranes that are equipped with an industrial hanging and crane scales for weighing heavy goods.

Fig. 5 shows the structure of the ANN based on the feedforward neural network adopted in this work. The structure is 2-3-2 that comprises of two input layer neurons, three hidden layer neurons and two output layer neurons. Each neuron in the layers is interconnected by a parameter known as weight. The indices i, j and k denote to neurons in the input, hidden and output layers, respectively. The input layer consists of input neurons ($x_i = 1, \ldots, u$) that accepts input signal (cable length and payload mass) in real time and redistributes these signals to all neurons in the hidden layer. Then, the actual outputs of the neurons in the hidden layer can be computed as

$$y_j = sigmoid\left[\sum_{i=1}^{u} x_i w_{ij} - \theta_j\right] \tag{11}$$

where u is the number of neurons in the input layer, *sigmoid* is the sigmoid activation function and w_{ij} is the weight that linked between the neuron i in the input layer and neuron j in the hidden layer. The threshold/bias applied to each of the hidden neuron is represented as θ_j, connected to a fixed input of -1. The actual outputs of the neurons in the output layer can be calculated as

$$y_k = sigmoid\left[\sum_{j=1}^{q} x_{jk} w_{jk} - \theta_k\right] \tag{12}$$

where q is the number of neurons in the hidden layer, w_{jk} and x_{jk} are the weight and input between neuron j in the hidden layer and neuron k in the output layer respectively. The parameter θ_k denotes the bias of the neuron in the output layer.

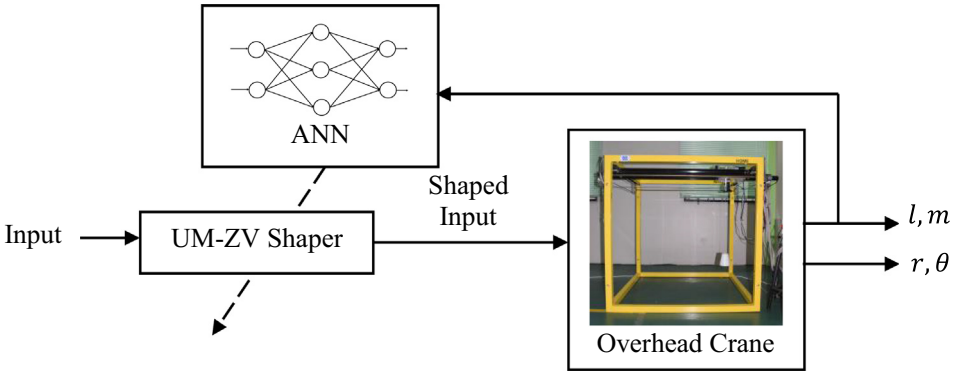

Fig. 4. ANN based input shaping control structure.

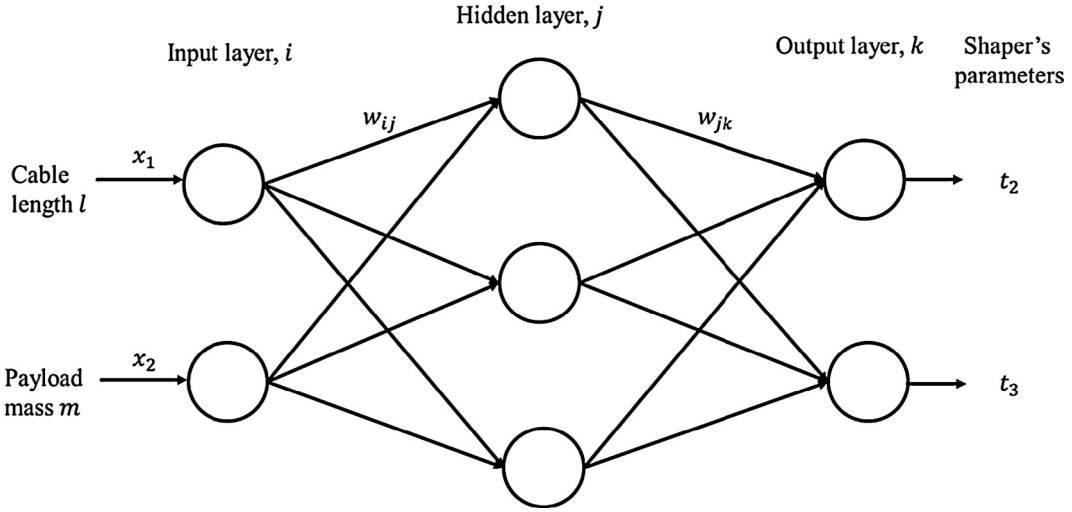

Fig. 5. Structure of the ANN.

To train the ANN, PSO algorithm was chosen as it offers a robust global search algorithm as compared to the conventional method namely the backpropagation algorithm where the convergence rate of the algorithm is slow and easily get trapped in local minima [43]. PSO has been a solution to several complex nonlinear optimisations by inspiring the concept/behaviour of bird flocking and fish schooling [44]. The control variables of the PSO were assigned as weights and biases of the ANN which correspond to the position vector of the i^{th} particle in the search space. The range for each control variable was assigned between [−10,10]. The population size of PSO was set as 40. To begin the training process, the position of a group of particles in the swarm was randomly initialised. Each particle can be assigned as a point in a *D*-dimensional space and their positions will be updated corresponding to the given velocity update to finally reach an optimal solution in the search space area. There are two best values called personal best, *pb* and global best, *gb* where the personal best is the best solution reached so far, while the global best is the overall best solution in the population.

The velocity of the i^{th} particle is given by

$$V_{id}^{t+1} = \omega V_{id}^{t} + c_1 r_{1d}^{t}[pb_{id}^{t} - x_{id}^{t}] + c_2 r_{2d}^{t}[gb_{d}^{t} - x_{id}^{t}] \tag{13}$$

$$x_{id}^{t+1} = x_{id}^{t} + v_{id}^{t+1} \tag{14}$$

where $d \in [1, D]$, $i \in [1, k]$ and t is the current iteration number. The parameters, c_1 and c_2 are the acceleration coefficients that were set as 1.5. The random numbers, r_1 and r_2 were assigned between [0,1]. The second term on the right side of Eq. (13) plays a role as a cognitive element which is beneficial to create an individual memory of the best position, gone through by the particle. Meanwhile, the last term forms a social interaction so that every particle could hover towards the best position reached by their neighbour. Hence, the presence of acceleration coefficients multiplied with the random values will maintain the stochastic influence for both cognitive and social components with the aim that all particles will get attracted to the average of both personal best and global best. Setting $c_1 = c_2$ will make the particles attract and influence on the average of personal best and global best. ω is the inertia weight that controls the momentum and the capability in terms of exploration and exploitation of the particles toward finding a good optimal place so that they would not diverge or going beyond the search space. Hence, ω was set with a large value at the beginning of the iteration for particles to explore freely in the entire swarm (exploration) and decreased linearly with the iteration number to achieve a quick convergence and able to search around the target point (exploitation). To satisfy this, ω was set as

$$\omega^{t+1} = \omega_{max} - \left(\frac{\omega_{max} - \omega_{min}}{t_{max}}\right) t \tag{15}$$

where ω_{max} and ω_{min} are the maximum and minimum values of inertia weight that were set as 0.9 and 0.4, respectively. t_{max} is the maximum iteration number. All particles were evaluated based on its corresponding fitness value, *J* which is based on mean square error (MSE), given as

$$J = \frac{1}{2b}\sum_{s=1}^{b}\sum_{k=1}^{p}(yd_k(s) - y_k(s))^2 \tag{16}$$

where b and p denote the number of training sample and the number of output neurons respectively. $yd_k(s)$ and $y_k(s)$ are the desired and actual outputs for the s^{th} sample at the k^{th} neuron of output layer, respectively. The fitness value of each particle will be calculated in every iteration to update the pb and gb values. The fitness of each particle was compared with the personal best reached so far, in which the fittest value will be assigned as a new personal best. Moreover, the fitness value of each particle is compared with the global best value and the better one will take place as a new global best. Each particle position is updated by its current velocity until all the particles have converged and optimal solution has been achieved. In this problem, the aim of PSO is to train the ANN so that the particles (weights and biases) are adjusted to minimise the fitness value and to develop the required network mapping.

4.1. Analysis of the ANN training results

Three-fourth of the collected data (Table 2) were selected randomly as training data and the rest of the data, which were samples number 3, 10, 13, 16, 20, 26 and 30 were used as testing data to evaluate the validity and reliability of the network mapping. By obtaining a good network mapping, with any new input (cable length and payload mass) that are measured during the real time crane operation, optimal shaper's parameters can be predicted and the UMZV shaper can thus be updated. The fitness value as calculated in Eq. (16) for the training data which was processed by PSO is shown in Fig. 6. It was noted that PSO managed to train the ANN in solving the minimisation problem and achieved approximately zero fitness value indicating that the network has converged. The set of final weights and biases obtained using the algorithm are shown in Table 3.

In this work, several performance indices were used to evaluate the performance of the ANN model. These include the relative error (δ_i), prediction accuracy (PA) and coefficient of determination (R^2), given as

$$\delta_i = \frac{|t_i' - t_i|}{t_i} \times 100\% \tag{17}$$

$$PA = 100\% - \frac{1}{n}\sum_{i=1}^{n} \frac{|t_i' - t_i|}{t_i} \times 100\% \tag{18}$$

$$R^2 = 1 - \frac{\sum_{i=1}^{n}(t_i' - t_i)^2}{\sum_{i=1}^{n}(t_i - T)^2} \tag{19}$$

where t_i and t_i' indicate the actual and prediction values of the shaper's parameters, t_2 or t_3, respectively while T is the mean value of t_i. The parameter n is the number of testing samples that is equal to 7.

Table 4 shows the relative errors between the actual and predicted values of the UMZV parameters. The maximum numbers of the relative error of t_2 and t_3 were noted as 9.204% and 5.4613% respectively. Besides, the PA values of t_2 and t_3 were

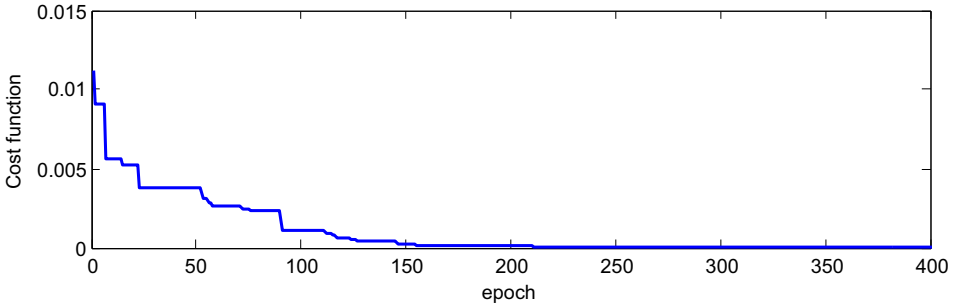

Fig. 6. Relationship between epoch and the fitness value during the training process.

Table 3
The weights and biases of ANN.

The weights between the input and hidden layers w_{ij}						The biases in the hidden layer θ_j		
w_{11}	w_{12}	w_{13}	w_{21}	w_{22}	w_{23}	θ_1	θ_2	θ_3
−7.1048	4.8275	10	−0.1354	−0.1630	10	1.4745	5.7060	−2.2843
The weights between the hidden and output layers w_{jk}						The biases in the output layer θ_k		
w_{11}	w_{12}	w_{21}	w_{22}	w_{31}	w_{32}	θ_1		θ_2
−8.2670	−10	6.4146	10	−5.1801	−9.4777	−3.8218		−9.0687

Table 4
Prediction errors.

Sample no.	3	10	13	16	20	26	30
t_2	0.186	0.2119	0.11	0.2089	0.153	0.148	0.2814
t_2'	0.1853	0.2098	0.1088	0.2095	0.1544	0.1555	0.2555
δ	0.3763%	0.9910%	1.0909%	0.2872%	0.9150%	5.0676%	9.204%
t_3	0.3724	0.4242	0.2179	0.4234	0.3027	0.3	0.542
t_3'	0.3717	0.4199	0.2143	0.4190	0.3089	0.3109	0.5124
δ	0.188%	1.0137%	1.6521%	1.0392%	2.0482%	3.6333%	5.4613%

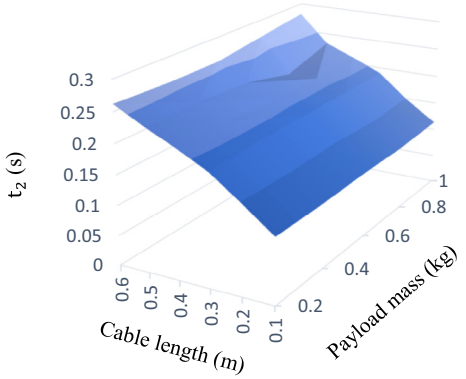

Fig. 7. Effect of cable length and payload mass on t_2 parameter.

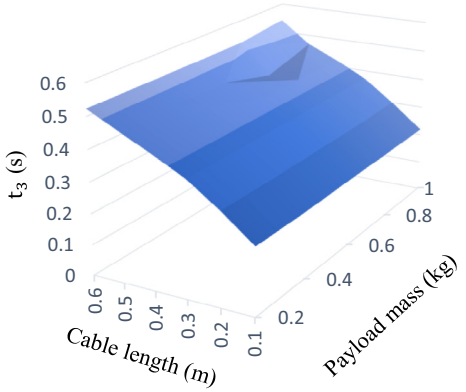

Fig. 8. Effect of cable length and payload mass on t_3 parameter.

calculated as 97.44% and 97.85%, respectively which show good generalisation ability. Furthermore, the R^2 criterion in training for both t_2 and t_3 are 0.9605 and 0.9839, respectively indicating no significant different between the actual and the prediction results. With the higher accuracy and less relative errors, the developed network mapping can be considered reliable to be used for prediction in the real time crane operation with time-varying parameters.

Using the mapping, the effects of the cable length and payload mass on the UMZV parameters, t_2 and t_3 are shown in Fig. 7 and Fig. 8 respectively. It was found that the cable length has a great influence on both parameters, while the effect of the payload mass was relatively small. Hence, this proves that a scheme that can update the shaper parameters is required for a uniform system performance especially during the hoisting operation.

5. Implementation and results

This section presents the real-time implementations on the laboratory overhead crane using the proposed ANN-based UMZV shaper (ANN-UMZV), UMZV shaper designed using an average operating frequency (AOF-UMZV), ZVDD shaper and ZVDD shaper with varying frequency (VF-ZVDD). The analysis on the control performances were carried out to investigate

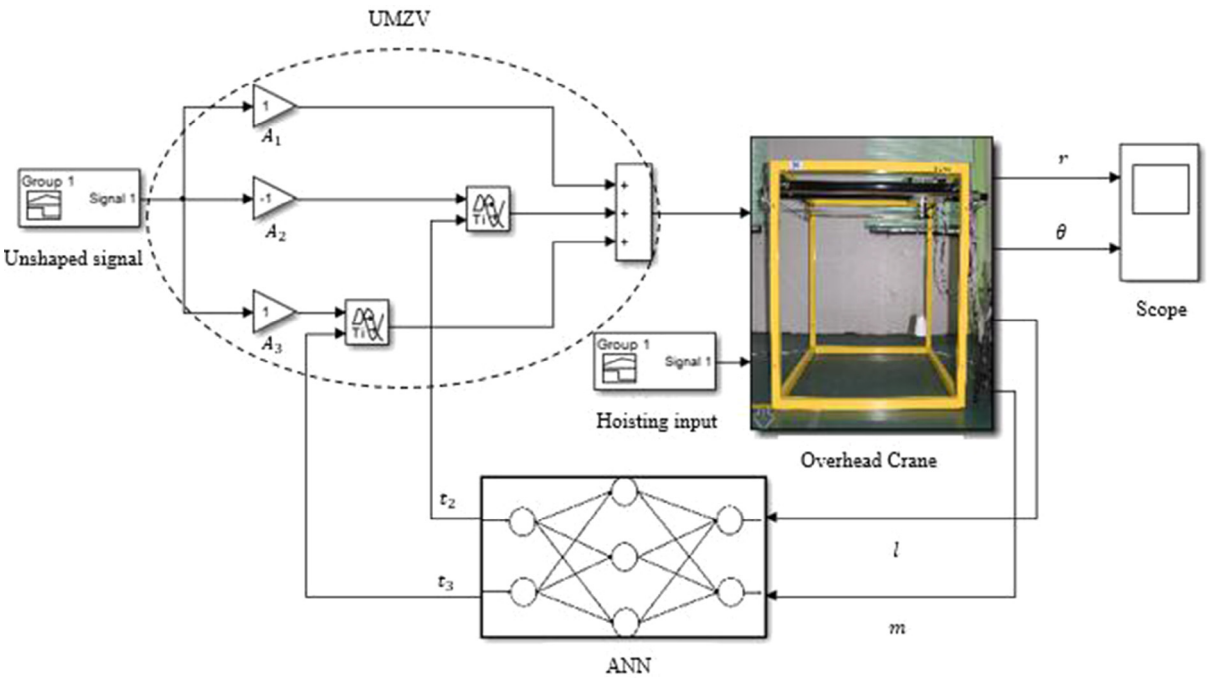

Fig. 9. ANN-UMZV Simulink block.

the effectiveness of ANN-UMZV to reduce the induced payload swing due to simultaneous crane motions, payload hoisting and payload mass variations. A Simulink design of the ANN-UMZV for real time implementation is illustrated in Fig. 9.

Two different payload masses of 0.24 kg and 0.74 kg were used and they are of the same shape and size for a fair comparison. It is worth mentioning that the payload masses are different from the training and testing data, and therefore can be used to verify the controller performance. Due to the limitations of the laboratory crane and to achieve a fast motion, the payload was hoisted from 0.17 m to 0.59 m with a maximum velocity as shown in Fig. 10. In this condition, the frequency changed from 7.6 to 4.07 rad/s which indicate a decrement of 46.3%. Fig. 11 illustrates two input signals of the trolley used in this work, given as Input 1 and Input 2 that represent a finite actuated crane. Input 1 is a pulse signal with amplitude of 0.5 N for a period of 3 s, while Input 2 is a pulse signal with amplitudes of 0.5 N and 1 N to represent slow and fast motions. This is a typical signal applied by a crane operator where initially a crane is moved with a slow motion, then accelerate to a full velocity and eventually decelerate for an accurate payload positioning. Two experimental cases were considered, based on both inputs and different motions of trolley. These were:

- Case 1: Simultaneous motions of the trolley and payload hoisting with Input 1.
- Case 2: Simultaneous motions of the trolley and payload hoisting with Input 2.

For both cases, the trolley and the payload were set to reach the target at the same time, which is at 3 s for an optimal duration of the payload movement. The performances of the proposed ANN-UMZV over the AOF-UMZV and ZVDD shapers were analysed based on the level of the payload swing reductions and the transient and residual swing angles when the payload undergoes hoisting and changes in payload mass. As the objective is to achieve a zero payload swing, the mean square

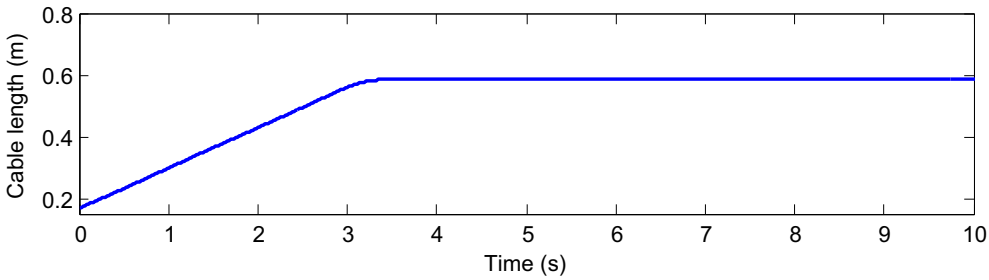

Fig. 10. Cable length hoisting.

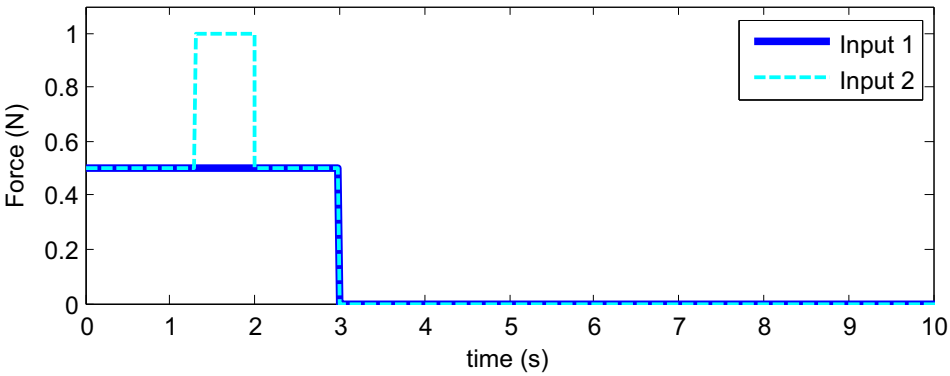

Fig. 11. Input signals of the trolley.

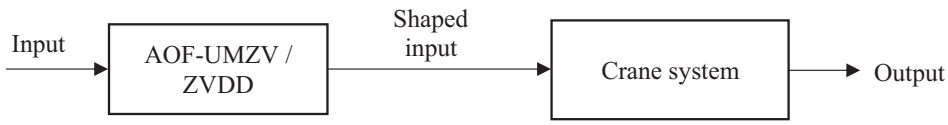

Fig. 12. A block diagram for implementations of AOF-UMZV and ZVDD shapers.

Table 5
Shaper's parameters of AOF-UMZV and ZVDD.

Parameters	ω_n (rad/s)	A_1	A_2	A_3	A_4	t_1 (s)	t_2 (s)	t_3 (s)	t_4 (s)
AOF-UMZV	5.84	1	−1	1	–	0	0.18	0.36	–
ZVDD	7.6	0.1310	0.3808	0.3690	0.1192	0	0.4136	0.8272	1.2408

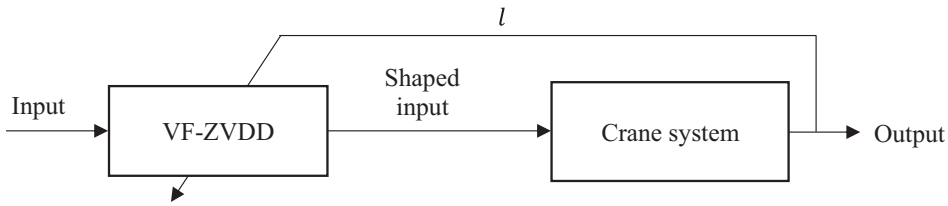

Fig. 13. A block diagram for implementations of VF-ZVDD shaper.

error (MSE) can be used as a performance index that represents overall swing, where a lower value of MSE indicates a higher swing suppression. Meanwhile, maximum transient swing (MT) and residual swing (RS) were also calculated in which low values of MT and RS are desirable. In this work, the RS was considered as a payload swing that is exhibited after a trolley has reached a steady-state value.

For performance comparisons, the AOF-UMZV and ZVDD shapers were designed and implemented in a feedforward scheme as shown in Fig. 12. With the payload hoisting between 0.17 m and 0.59 m, the ZVDD shaper was designed with a swing frequency of 7.6 rad/s and the AOF-UMZV with an average frequency of 5.84 rad/s. Based on several experiments, the system damping ratio was approximated as 0.01. By solving Eqs. (7) and (9), the AOF-UMZV and ZVDD shaper's parameters can be obtained as given in Table 5. Besides, the VF-ZVDD shaper was also implemented as shown in Fig. 13, where the shaper parameters can be updated online by measuring the cable length during payload hoisting. A linearised frequency [45] of the single pendulum dynamic can be calculated as $\omega = \sqrt{g/l}$.

5.1. The effects of payload hoisting and payload mass variations

The effects of hoisting and payload mass variations on the payload swing response of the laboratory overhead crane were firstly examined for both cases. Fig. 14 illustrates the swing responses without the input shaping while the calculated performance indices for all swing responses are shown in Table 6.

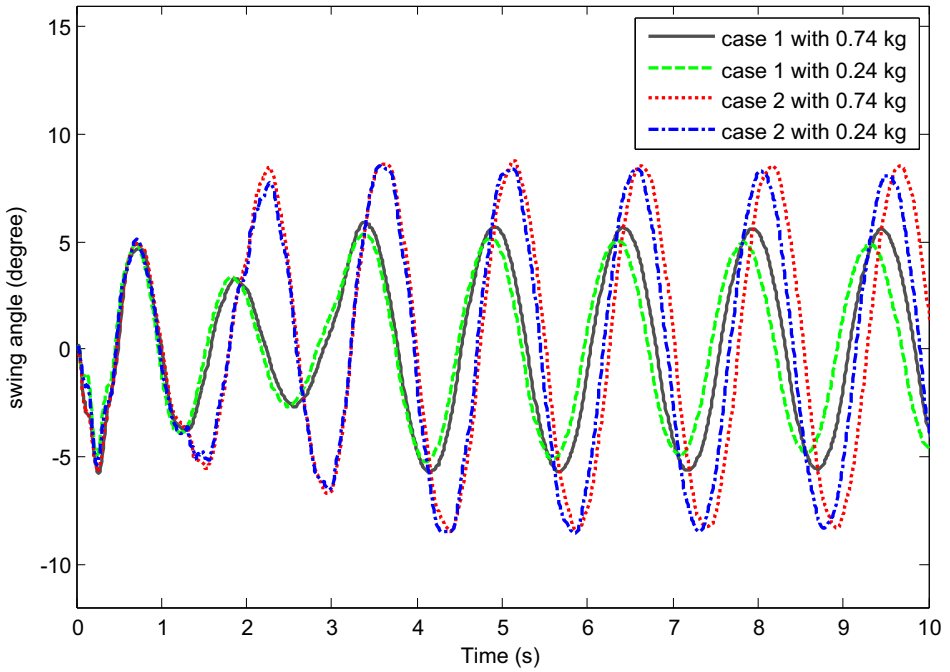

Fig. 14. Induced payload swing responses for Case 1 and Case 2 with payloads of 0.74 kg and 0.24 kg (without shaper).

Table 6
Performance indices of payload swing responses without input shaping.

Performance Index	Case 1		Case 2	
	0.24 kg payload	0.74 kg payload	0.24 kg payload	0.74 kg payload
MSE	10.894	14.434	30.512	32.446
MT	5.4013	5.8829	8.5744	8.7318

It was noted that the increase in the payload mass induced more payload swing as the MSE and MT values of the 0.74 kg payload for both cases were higher as compared to the 0.24 kg payload. It was also found that the maximum swing angle for Case 2 was significantly higher than that of Case 1. For both payloads, the MSE and MT values increased more than 120% and 50%, respectively. This indicates that the changes between the slow and fast crane motions in Case 2 contributes to a significant impact on the induced payload swing.

5.2. Experimental results with input shapers

Figs. 15 and 16 illustrate the swing responses of the ANN-UMZV, AOF-UMZV and ZVDD shapers with payloads of 0.74 kg and 0.24 kg, respectively for Case 1. The MSE, MT and RS values for all the techniques are given in Fig. 17. Based on the overall swing (MSE) results, all shapers were capable to suppress the induced swing angle as compared to the unshaped response at least by 90.74% and 89.81% reductions for the payloads of 0.74 kg and 0.24 kg, respectively. Further investigations showed that the proposed ANN-UMZV was superior than the other shapers, where the ANN-UMZV recorded in the lowest MSE and RS values, followed by the AOF-UMZV and ZVDD for both payload masses. This proved that the ANN-UMZV can greatly eliminate the swing response, in which a nearly zero RS was obtained. The ZVDD shaper was shown to provide the lowest MT over the other shapers, however with an unsatisfactory RS.

For Case 2, Figs. 18 and 19 illustrate the payload swing responses of the crane utilising all the shapers for the payloads of 0.74 kg and 0.24 kg, respectively. The MSE results calculated for all the shapers show swing reductions of at least 91.78% and 93.15% as compared to the unshaped response was achieved for the payloads of 0.24 kg and 0.74 kg respectively as shown in Fig. 20. The ANN-UMZV was shown to be the best shaper with improvements of at least 60.6% and 38.9% of the MSE values as compared to the AOF-UMZV and ZVDD shapers respectively. The RS performance of the ANN-UMZV in Case 2 also showed to be proficient when eliminating the residual swing significantly with 100% and 91.3% suppressions for payloads of 0.74 kg and 0.24 kg, respectively as compared to the other shapers. However, in terms of MT, the ZVDD attained the smallest result over the others but it was incompetent to eliminate the RS as achieved by the ANN-UMZV. In Case 1, the AOF-UMZV overall

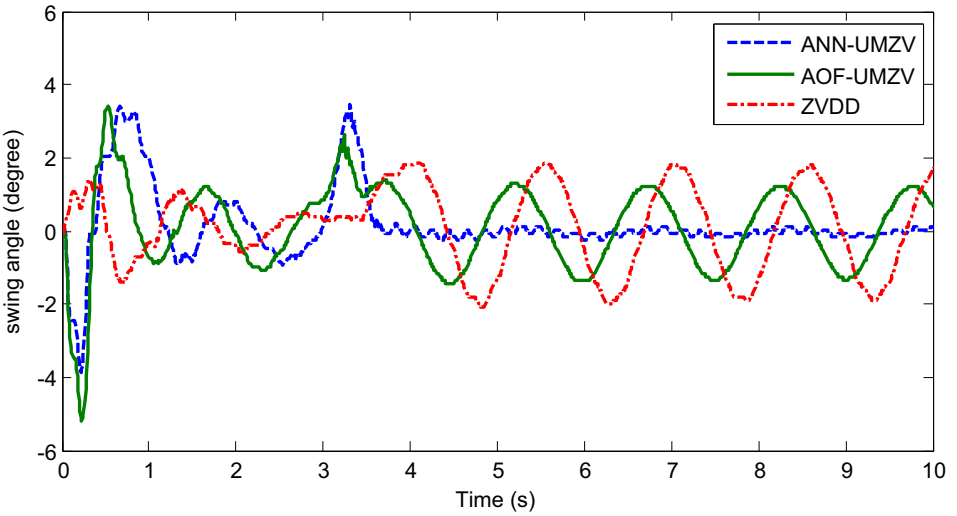

Fig. 15. Payload swing responses of the crane for Case 1 with payload mass of 0.74 kg.

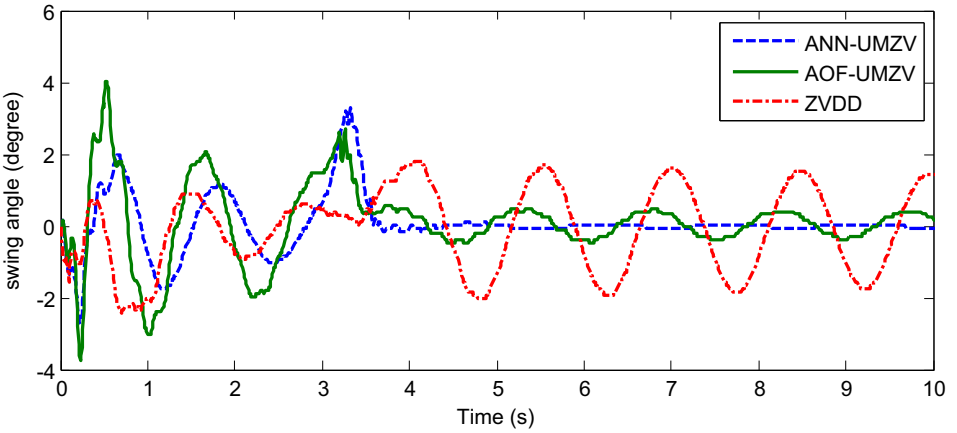

Fig. 16. Payload swing responses of the crane for Case 1 with payload mass of 0.24 kg.

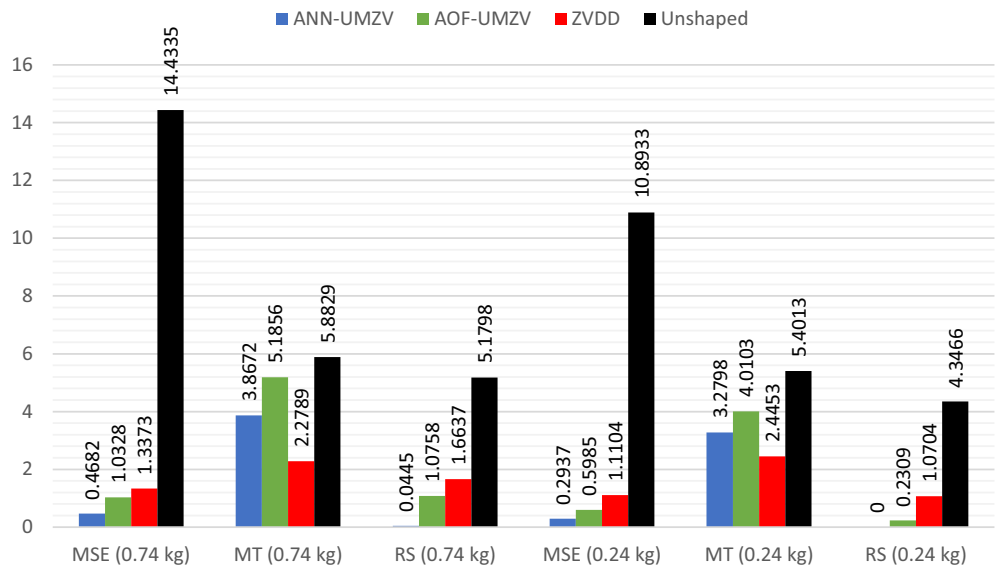

Fig. 17. Performance criterions of the payload swing responses for Case 1.

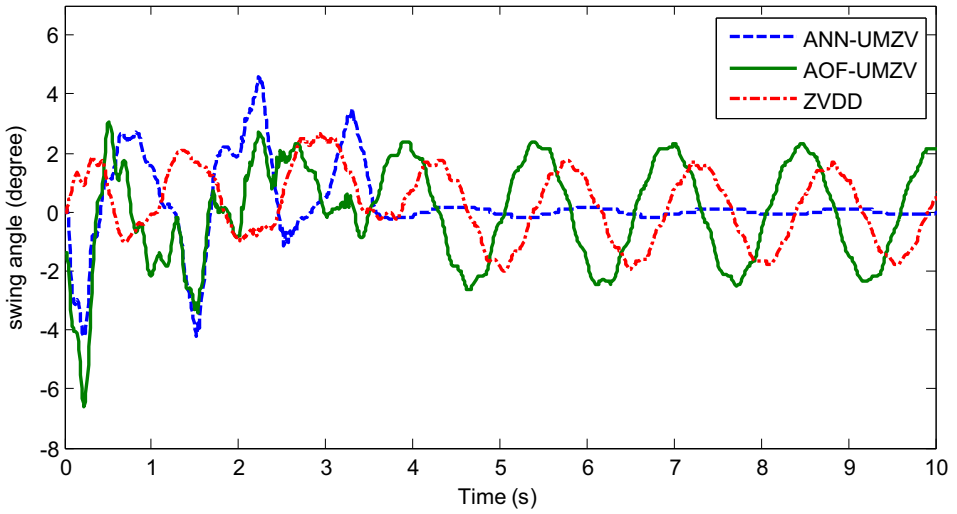

Fig. 18. Payload swing responses of the crane for Case 2 with payload mass of 0.74 kg.

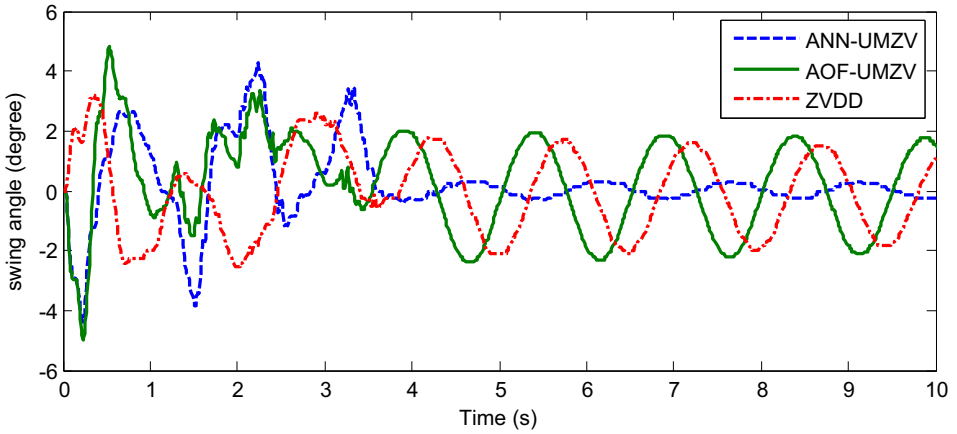

Fig. 19. Payload swing responses of the crane for Case 2 with payload mass of 0.24 kg.

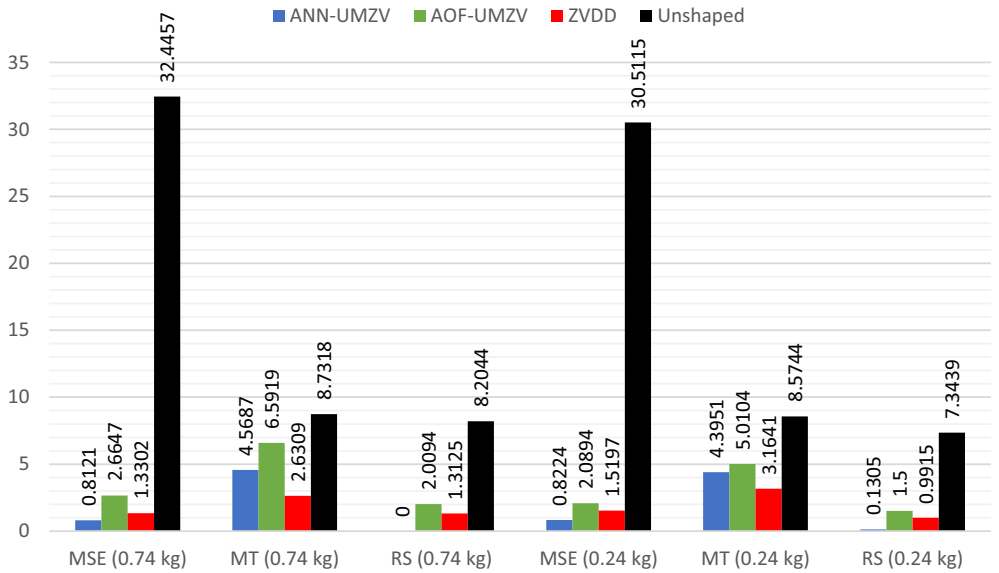

Fig. 20. Performance criterions of the payload swing responses for Case 2.

performance results (MSE) were better than the ZVDD, however as recorded in Case 2, the ZVDD performances was superior than that of the AOF-UMZV in all performance criterions for both payload masses. Also, it is worth mentioning that the proposed ANN-UMZV shaper was capable to provide a uniform performance under various conditions involving payload hoisting and payload mass. Fig. 21 shows the variations of the UMZV shaper's parameters (t_2 and t_3) during the crane motions, which proved that the proposed shaper is capable to predict and update the shaper to handle parameter varying effects.

Figs. 22 and 23 illustrate the trolley position responses for Case 1 and Case 2 respectively with both payloads. The trolley moved to a longer distance in Case 2 as Input 2 has more energy as shown in Fig. 11. With different shaping techniques used to shape the input signal, the final trolley positions were found to be slightly difference. It was also noted that the UMZV shapers provided a faster trolley response as compared to the ZVDD shaper. In these investigations, the shaper durations were also examined as this corresponds to the speed of response. Fig. 24 shows the shaper durations and residual swing for all the shapers and under all testing conditions. Obviously, the residual responses for the unshaped input (without shaper) were the worst and the crane stopped within 3 s. It was noted that in terms of the RS, the ANN-UMZV shaper outperformed the ZVDD and AOF-UMZV shapers in all conditions with almost a similar performance. For the shaper duration, it was shown that the AOF-UMZV shaper was slightly faster than the ANN-UMZV, nevertheless with higher residual swing angles.

Fig. 25 shows the payload swing responses of the overhead crane using the VF-ZDDD shaper with both payloads for Case 2. Besides providing a higher swing, this experimental case (Case 2) was examined as this is a typical command used by crane operators. With a payload of 0.74 kg, MSE, MT and RS were achieved as 0.8593, 2.8125 and 0.9395 respectively. On the other hand, for a payload of 0.24 kg, the values were obtained as 0.8389, 2.7246 and 0.5363. By comparing with the results in Fig. 20, it was noted that the MT of VF-ZVDD is 38% lower than ANN-UMZV. However, the proposed ANN-UMZV shaper achieved 5.8% and 2.0% lower in the overall swing for payloads of 0.74 kg and 0.24 kg respectively. More

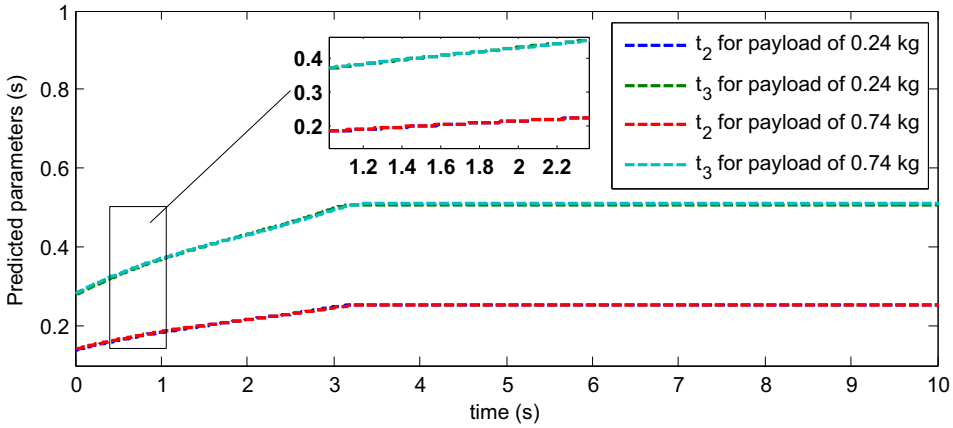

Fig. 21. The predicted t_2 and t_3 based on the ANN-UMZV during crane operation.

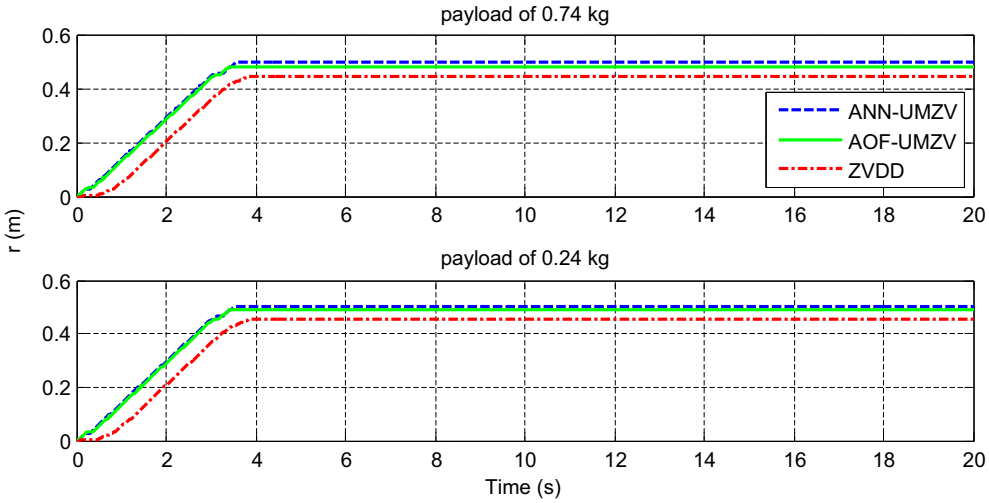

Fig. 22. Trolley moving distance for Case 1.

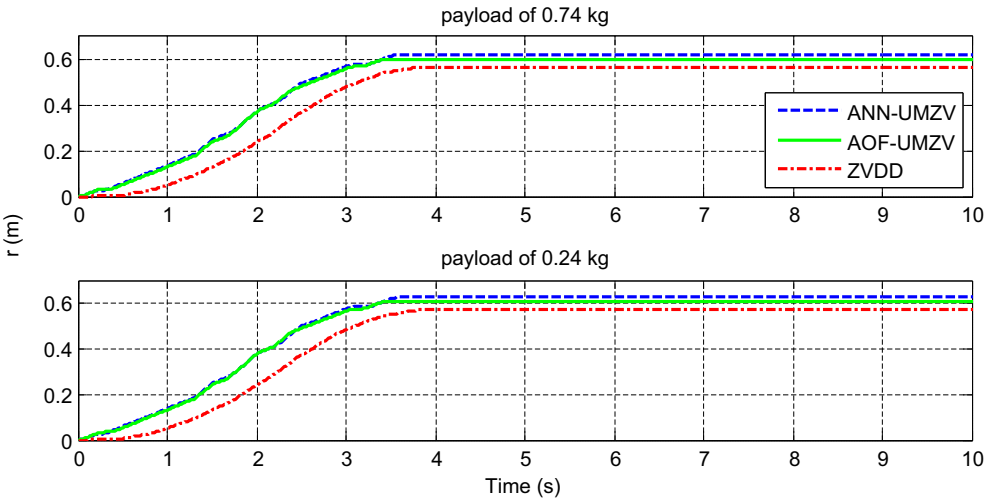

Fig. 23. Trolley moving distance for Case 2.

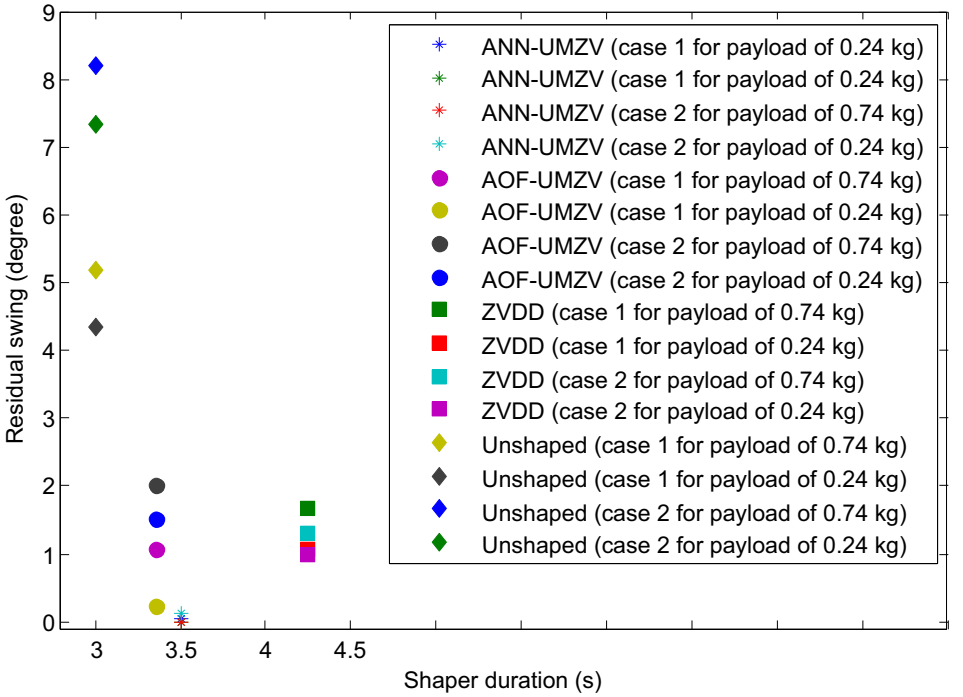

Fig. 24. Shaper durations and residual swing using all techniques.

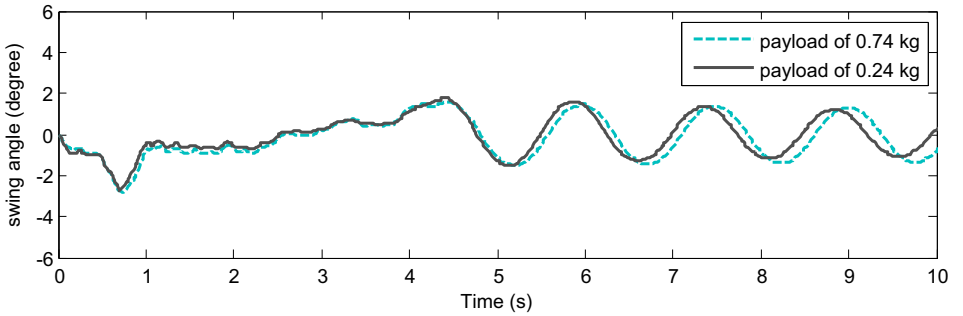

Fig. 25. Payload swing responses for payloads of 0.74 kg and 0.24 kg.

importantly, the residual swing with the ANN-UMZV shaper is significantly small and settle down faster. As expected, the VF-ZVDD shaper showed better performance in all criterions as compared to the ZVDD shaper with a fixed frequency.

For the implementation, as the ANN and PSO algorithms were used, the proposed shaper required more computational loads as compared to the traditional input shapers. However, the proposed UMZV shaper might be desirable as it was shown to achieve a fast response together with higher payload swing suppressions of the nonlinear overhead crane. Besides the cable length variations, the changes in the payload mass can also be considered. Despite producing finite actuation states, the ANN-UMZV was efficient in swing suppression of the overhead crane when compared to the robust shaper (ZVDD) that produced infinite actuation states.

6. Conclusion

An improved UMZV shaper based on ANN was designed and implemented in real time for payload swing reductions of an overhead crane with hoisting effect and payload mass variations. For performance comparisons, the UMZV based on AOF, and the robust shapers (ZVDD) based on fixed and varying frequencies were implemented. Experimental results showed that the ANN-UMZV achieved the highest reductions in the overall and residual swing, indicating that the technique is capable to predict and update the shaper parameters and handle those effects. Almost a similar performance was achieved under various testing conditions. The proposed technique can be beneficial for crane systems with finite actuation states and has an advantage of a shorter shaper duration and fast response. The PSO and ANN methods can also be utilised for other shapers in determining the optimal number of impulses, time locations and amplitudes with the presence of uncertainties.

Acknowledgement

The authors gratefully acknowledged Universiti Teknologi Malaysia, Malaysia for the financial support through Research University Grant Vote No. 14J06.

References

[1] W. Singhose, L. Porter, M. Kenison, E. Kriikku, Effects of hoisting on the input shaping control of gantry cranes, Control Eng. Pract. 8 (2000) 1159–1165.
[2] L. Ramli, Z. Mohamed, A.M. Abdullahi, H.I. Jaafar, I.M. Lazim, Control strategies for crane systems: A comprehensive review, Mech. Syst. Signal Process. 95 (2017) 1–23.
[3] D. Fujioka, M. Shah, W. Singhose, Robustness analysis of input-shaped model reference control on a double-pendulum crane, in: 2015 Am. Control Conf., IEEE, Chicago, 2015, pp. 2561–2566.
[4] S. Garrido, M. Abderrahim, A. Gimenez, R. Diez, C. Balaguer, Anti-swinging input shaping control of an automatic construction crane, IEEE Trans. Autom. Sci. Eng. 5 (2008) 549–557.
[5] Z.N. Masoud, M.F. Daqaq, A graphical approach to input-shaping control design for container cranes with hoist, IEEE Trans. Control Syst. Technol. 14 (2006) 1070–1077.
[6] W. Singhose, J. Vaughan, Reducing vibration by digital filtering and input shaping, IEEE Trans. Control Syst. Technol. 19 (2011) 1410–1420.
[7] J. Vaughan, J. Yoo, N. Knight, W. Singhose, Multi-input shaping control for multi-hoist cranes, in: 2013 Am. Control Conf., Washington, USA, 2013, pp. 3455–3460.
[8] M.J. Maghsoudi, Z. Mohamed, A.R. Husain, M.O. Tokhi, An optimal performance control scheme for a 3D crane, Mech. Syst. Signal Process. 66–67 (2016) 756–768.
[9] A.M. Abdullahi, Z. Mohamed, H. Selamat, H.R. Pota, M.S.Z. Abidin, F.S. Ismail, A. Haruna, Adaptive output-based command shaping for sway control of a 3D overhead crane with payload hoisting and wind disturbance, Mech. Syst. Signal Process. 98 (2018) 157–172.
[10] K.A. Alhazza, Adjustable maneuvering time wave-form command shaping control with variable hoisting speeds, J. Vib. Control. 23 (2017) 1095–1105.
[11] M.J. Maghsoudi, Z. Mohamed, S. Sudin, S. Buyamin, H.I. Jaafar, An improved input shaping design for an efficient sway control of a nonlinear 3D overhead crane with friction, Mech. Syst. Signal Process. 92 (2017) 364–378.
[12] M.O.T. Cole, T. Wongratanaphisan, A direct method of adaptive FIR input shaping for motion control with zero residual vibration, IEEE/ASME Trans. Mechatronics. 18 (2013) 316–327.
[13] M.A. Ahmad, M.S. Ramli, R.M.T. Raja Ismail, Infinite impulse response filter techniques for sway control of a lab-scaled rotary crane system, in: 2010 Int. Conf. Comput. Model. Simul. (ICCMS 2010), Sanya, China, 2010, pp. 192–196.
[14] X. Xie, J. Huang, Z. Liang, Vibration reduction for flexible systems by command smoothing, Mech. Syst. Signal Process. 39 (2013) 461–470.
[15] J. Huang, X. Xie, Z. Liang, Control of bridge cranes with distributed-mass payload dynamics, IEEE/ASME Trans. Mechatronics. 20 (2015) 481–486.
[16] J. Huang, Z. Liang, Q. Zang, Dynamics and swing control of double-pendulum bridge cranes with distributed-mass beams, Mech. Syst. Signal Process. 54 (2015) 357–366.
[17] M.I. Solihin, Wahyudi, M.A.S. Kamal, A. Legowo, Optimal PID controller tuning of automatic gantry crane using PSO algorithm, in: Proceeding 5th Int. Symp. Mechatronics Its Appl. (ISMA 2008), Jordan, 2008, pp. 1–5.
[18] H.I. Jaafar, S.Y.S. Hussien, R. Ghazali, Optimal tuning of PID + PD controller by PFS for gantry crane system, in: 2015 10th Asian Control Conf., Sabah, Malaysia, 2015, pp. 1–6.
[19] Q.H. Ngo, N.P. Nguyen, C.N. Nguyen, T.H. Tran, K.S. Hong, Fuzzy sliding mode control of container cranes, Int. J. Control. Autom. Syst. 13 (2015) 419–425.
[20] D. Qian, J. Yi, Hierarchical Sliding Mode Control for Under-Actuated Cranes, Springer, Berlin Heidelberg, 2015.
[21] H. Chen, Y. Fang, S. Member, N. Sun, A swing constraint guaranteed MPC algorithm for underactuated overhead cranes, IEEE/ASME Trans. Mechatronics. 21 (2016) 2543–2555.
[22] J. Smoczek, J. Szpytko, Particle swarm optimization-based multivariable generalized predictive control for an overhead crane, IEEE/ASME Trans. Mechatronics. 22 (2016) 258–268.
[23] J. Smoczek, Experimental verification of a GPC-LPV method with RLS and P1-TS fuzzy-based estimation for limiting the transient and residual vibration of a crane system, Mech. Syst. Signal Process. 62–63 (2015) 324–340.
[24] N. Sun, Y. Fang, H. Chen, Adaptive antiswing control for cranes in the presence of rail length constraints and uncertainties, Nonlinear Dyn. 81 (2015) 41–51.
[25] M. Zhang, X. Ma, X. Rong, X. Tian, Y. Li, Adaptive tracking control for double-pendulum overhead cranes subject to tracking error limitation, parametric uncertainties and external disturbances, Mech. Syst. Signal Process. 76–77 (2016) 15–32.

[26] J. Smoczek, Fuzzy crane control with sensorless payload deflection feedback for vibration reduction, Mech. Syst. Signal Process. 46 (2014) 70–81.
[27] C.Y. Chang, Adaptive fuzzy controller of the overhead cranes with nonlinear disturbance, IEEE Trans. Ind. Informatics. 3 (2007) 164–172.
[28] N. Sun, Y. Wu, H. Chen, Y. Fang, An energy-optimal solution for transportation control of cranes with double pendulum dynamics: Design and experiments, Mech. Syst. Signal Process. 102 (2018) 87–101.
[29] W. Singhose, Command shaping for flexible systems: A review of the first 50 years, Int. J. Precis. Eng. Manuf. 10 (2009) 153–168.
[30] C.F. Cutforth, L.Y. Pao, Adaptive input shaping for maneuvering flexible structures, Automatica 40 (2004) 685–693.
[31] A. Tzes, S. Yurkovich, An adaptive input shaping control Scheme for vibration suppression in slewing flexible structures, IEEE Trans. Control Syst. Technol. 1 (1993) 114–121.
[32] M. Bodson, An adaptive algorithm for the tuning of two input shaping methods, Automatica 34 (1998) 771–776.
[33] J. Park, P.H. Chang, Learning input shaping technique for non-LTI systems, Proc. Am. Control Conf. 5 (1998) 2652–2656.
[34] K.L. Sorensen, K. Hekman, W.E. Singhose, Finite-state input shaping, IEEE Trans. Control Syst. Technol. 18 (2010) 664–672.
[35] S.S. Gurleyuk, Optimal unity-magnitude input shaper duration analysis, Arch. Appl. Mech. 77 (2007) 63–71.
[36] W.P. Seering, N.C. Singer, Time-optimal negative input shapers, J. Dyn. Syst. Meas. Control. 119 (1997).
[37] L.Y. Pao, W.E. Singbose, Unity-magnitude input shapers and their relation to time-optimal control, in: 13th Trienn. World Congr., San Francisco, USA, 1996, pp. 385–390.
[38] S.S. Gürleyük, Designing unity magnitude input shaping by using PWM technique, Mechatronics 21 (2011) 125–131.
[39] W.P. Seering, Preshaping command inputs to reduce system vibration, J. Dyn. Syst. Meas. Control. 112 (1990) 76–82.
[40] L. Behera, I. Kar, Intelligent Systems and Control-principles and Applications, Oxford University Press, 2009.
[41] L.C. Jain, M. Seera, C.P. Lim, P. Balasubramaniam, A review of online learning in supervised neural networks, Neural Comput. Appl. 25 (2014) 491–509.
[42] M.M. Esfahani, A. Sheikh, O. Mohammed, Adaptive real-time congestion management in smart power systems using a real-time hybrid optimization algorithm, Electr. Power Syst. Res. 150 (2017) 118–128.
[43] D.J. Armaghani, M. Hajihassani, E.T. Mohamad, A. Marto, S.A. Noorani, Blasting-induced flyrock and ground vibration prediction through an expert artificial neural network based on particle swarm optimization, Arab. J. Geosci. (2014) 5383–5396.
[44] L. Ramli, Y. Sam, Z. Mohamed, M.K. Aripin, M.F. Ismail, Composite nonlinear feedback control with multi-objective particle swarm optimization for active front steering system, J. Teknol. 72 (2015) 13–20.
[45] K. Sorensen, W. Singhose, S. Dickerson, A controller enabling precise positioning and sway reduction in cranes with on-off actuation, Control Eng. Pract. 15 (2007) 825–837.